Hybrid functional investigations of band gaps and band alignments for AlN, GaN, InN, and InGaN

Poul Georg Moses, Maosheng Miao, Qimin Yan, and Chris G. Van de Walle

---

Articles you may be interested in

Hybrid functional investigations of band gaps and band alignments for AlN, GaN, InN, and InGaN

Poul Georg Moses,[a)] Maosheng Miao, Qimin Yan, and Chris G. Van de Walle
Materials Department, University of California, Santa Barbara, California 93106-5050, USA

Band gaps and band alignments for AlN, GaN, InN, and InGaN alloys are investigated using density functional theory with the with the Heyd–Scuseria–Ernzerhof {HSE06 [J. Heyd, G. E. Scuseria, and M. Ernzerhof, J. Chem. Phys. **134**, 8207 (2003); **124**, 219906 (2006)]} XC functional. The band gap of InGaN alloys as a function of In content is calculated and a strong bowing at low In content is found, described by bowing parameters 2.29 eV at 6.25% and 1.79 eV at 12.5%, indicating the band gap cannot be described by a single composition-independent bowing parameter. Valence-band maxima (VBM) and conduction-band minima (CBM) are aligned by combining bulk calculations with surface calculations for nonpolar surfaces. The influence of surface termination [($1\bar{1}00$) m-plane or ($11\bar{2}0$) a-plane] is thoroughly investigated. We find that for the relaxed surfaces of the binary nitrides the difference in electron affinities between m- and a-plane is less than 0.1 eV. The absolute electron affinities are found to strongly depend on the choice of XC functional. However, we find that *relative* alignments are less sensitive to the choice of XC functional. In particular, we find that relative alignments may be calculated based on Perdew–Becke–Ernzerhof [J. P. Perdew, K. Burke, and M. Ernzerhof, Phys. Rev. Lett. **134**, 3865 (1996)] surface calculations with the HSE06 lattice parameters. For InGaN we find that the VBM is a linear function of In content and that the majority of the band-gap bowing is located in the CBM. Based on the calculated electron affinities we predict that InGaN will be suited for water splitting up to 50% In content. © *2011 American Institute of Physics*. [doi:10.1063/1.3548872]

I. INTRODUCTION

Alloys of AlN [reported experimental band gap ranging from 6.11 (Ref. 1) to 6.2 eV (Refs. 2 and 3)], GaN [3.51 eV (Ref. 4)], and InN [0.6–0.7 eV (Refs. 5–9)] and heterostructures based on these nitrides are utilized in a growing number of applications such as light-emitting diodes (LED), laser diodes, and high electron mobility transistors (HEMT). Furthermore, alloys of InN and GaN have recently attracted interest for use in multijunction photovoltaic devices[10–12] and as photoelectrodes for water splitting.[13–20]

In photochemical water splitting, the InGaN semiconductor absorbs sunlight and thereby produces electrons and holes, which drives the water-splitting reaction. Successful photoelectrode materials must fulfill at least the following three criteria: (i) The band gap must be such that a significant fraction of the solar spectrum is absorbed; (ii) the conduction band (CB) and valence band (VB) must straddle the redox potential of hydrogen and water; and (iii) the material must be corrosion resistant. InGaN alloys have been found to fulfill these criteria and are, therefore, a potential candidate as a photoelectrode.[13–20] In the present study we focus on criteria (i) and (ii) and the materials properties of interest are, therefore, the band gap and band alignments.

The band alignments of GaN, InN, and InGaN alloys are key design parameters in optoelectronic devices and for

photochemistry. The VB offset between GaN and InN has been measured in a number of studies.[4,21–28] The most recent experimental study reported an offset of 0.58 ± 0.08 eV.[28] However, accurately measuring the offset is very difficult as seen from the wide spread (between 0.6 and 1.1 eV) of the reported experimental values.[21–28] Theoretical investigations using the linearized augmented plane wave (LAPW) method have reported values of 0.48 eV (Ref. 29) for wurtzite and 0.26 eV for zinc blende, recently revised to 1.11 eV (Ref. 30) for zinc blende. Plane-wave density functional theory (DFT) calculations have reported 0.3 eV (Ref. 31) for zinc blende, while empirical tight binding calculations of the branch point energies obtain 0.9 eV.[32]

Band offsets for AlN, GaN, and AlGaN alloys are also important for device applications such as lasers and HEMTs. The variation in reported experimental VB offsets is, again, quite large [0.15 (Ref. 33) to 1.4 eV (Refs. 32, 34, and 35)]. Theoretical investigations using linear muffin-tin orbitals produced an AlN/GaN VB offset of 0.85–1.15 eV,[36,37] while studies based on plane-wave DFT found values between 0.7 and 1.07 eV.[31,38–42] Quasiparticle studies based on the GW approximation yielded results in the range of 0.8–1.6 eV.[43,44] Some of this variation can be attributed to different choices of interface plane and different treatments of strain effects.

Experimental band gaps of the binary nitrides are well established, at least to within 0.1 eV: Reported values are 6.11 (Ref. 1) to 6.2 eV (Refs. 2 and 3) for AlN, 3.51 eV (Ref. 4) for GaN, and 0.6 to 0.7 eV (Refs. 5–8, and 9) for InN. For ternary nitride alloys, such as InGaN, consensus on the band gap as

---

a)Author to whom correspondence should be addressed. Electronic address: pgmoses@stanford.edu.

a function of composition has not been reached. A number of studies have measured the band gap as a function of In content,[45–53] resulting in a large spread in reported band gaps. Qualitatively, there is agreement that the band gap of InGaN is a nonlinear function of alloy composition. Conventionally, alloy band gaps are expressed as

$$E_g\left(In_xGa_{1-x}N\right) = (1-x)\,E_g^{GaN} + x\,E_g^{InN} - bx\,(1-x),$$
(1)

where x is the concentration of In and b is the so-called bowing parameter. The various experimental[45–53] as well as theoretical[54–64] studies have disagreed on the magnitude of the bowing parameter.

On the theory side, the standard methodology to perform first-principles calculations is based on DFT. It is well known that DFT consistently underestimates the band gap (the so-called "band-gap problem"). As a consequence, the positions of the valence and conduction bands (and hence the band offsets) also suffer from uncertainties. The band-gap problem has in a number of cases been addressed by *ad hoc* correction schemes. Typically, it has been assumed that VB offsets are affected less by the band-gap problem than conduction-band offsets. In the simplest correction scheme, the calculated VB offset is combined with experimental band gaps to produce a CB offset. There is no *a priori* justification, however, for assuming that the VB offset is accurately given by DFT. Empirically, the approximation was verified to work reasonably well (to within 0.2 eV) by comparing DFT results with quasiparticle calculations for conventional group IV, III–V, and II–VI compound semiconductors,[65,66] but in other cases [e.g., AlN/GaN nitrides[43] with a shift of 0.2–0.4 eV and Si/SiO$_2$ (Ref. [67])] larger shifts have been reported.

In principle, one way of addressing this issue is by combining DFT calculations for the structure and for the electrostatic potential lineup (which are ground-state properties) with quasiparticle calculations for the bulk material in the GW approach to obtain corrected positions of the bands with respect to the electrostatic potential.[65,66] In practice, several problems arise. First, GW calculations for nitride semiconductors are far from straightforward since they cannot simply be applied as a one-shot perturbation on top of standard DFT calculations, but require a better starting point than typically provided by the local density approximation (LDA) or generalized gradient approximation (GGA).[68–71] This renders this approach computationally very expensive, particularly when different alloy compositions need to be explored. Second, there is still uncertainty about exactly how to align the GW quasiparticle band structure with the DFT band structure. Specifically, it is not clear whether the DFT macroscopic averaged electrostatic potential is an appropriate reference for GW energy levels or whether a full GW calculation for the entire interface/surface is needed.[72] Because of these complications, we have chosen to pursue a different approach, based on hybrid functionals, in which there has recently been a lot of progress. Hybrid functionals of the PBE0 flavor have previously been used to investigate zinc blende InGaN alloys and were found to overestimate the band gap in the In-rich region, and lead to a GaN/InN offset of approximately 1.9 eV.[73]

In the present paper we use the Heyd–Scuseria–Ernzerhof (HSE06, Refs. [74] and [75]) exchange-correlation (XC) functional to address the band-gap problem. HSE06 requires significantly more computer resources than XC functionals based on the LDA or GGA, and, therefore, we judiciously evaluate which aspects of the problem specifically require the use of the more sophisticated functional. This will allow us to present guidelines on how to combine GGA and hybrid functionals to render the calculations computationally tractable. HSE06 produces significantly more accurate band gaps than LDA or GGA [we used the Perdew–Burke–Ernzerhof (PBE, Ref. [76]) flavor of GGA], but still slightly underestimates the gaps of AlN, GaN, and InN. The underestimation can be remedied by increasing the ratio of exact exchange mixed into the XC functional. However, the required amount of mixing to reproduce the exact experimental gaps is different for the three nitrides, and we, therefore, decided it was preferable to use the default 25% mixing. For InGaN alloys, we performed a thorough comparison of HSE06 band gaps with values calculated with LDA or PBE, and found that the latter produces results that match HSE06 to within 0.05 if a correction term is added that is a linear interpolation between the band-gap corrections for the binary compounds. A preliminary account of some of these findings was published in Ref. [77].

We find that *relative* natural band alignments can be obtained by calculating the potential alignment between bulk and vacuum with PBE, provided consistent lattice parameters are used (i.e., we consistently use the HSE06 lattice parameters). This procedure renders the calculations computationally tractable, particularly in the case of alloys.

Our VB alignments between the binary nitrides, calculated explicitly with HSE06, are found to be 0.34 eV for AlN/GaN and 0.62 eV for GaN/InN [we use the convention that a positive value for the VB offset for an A/B pair of materials indicates that the valence-band maxima (VBM) in B is higher in energy than the VBM in A]. VB alignments of InGaN are found to be a linear function of In content; i.e., all the band-gap bowing is found to be associated with the conduction-band minima (CBM). Based on the calculated positions of the VBM and CBM we predict that InGaN will be a suitable photochemical electrode for water splitting up to 50% In content.

II. CALCULATIONAL METHOD

The calculations are performed using the ASE software package[78] as an interface to VASP,[79,80] which is based on a plane-wave basis and projected augmented wave (PAW) potentials.[81,82] We use a plane-wave basis with an energy cutoff of 340 eV. For bulk calculations we use a coarse Fourier transform grid including three-fourths of the reciprocal vectors and a fine FFT grid representing the PAW potentials including two times the number of grid points in the coarse grid, i.e., the maximum number of grid points. For surface calculations we find that a coarse FFT grid including all of the reciprocal vectors is needed to obtain a smooth planar average of the electrostatic potential. We use a Γ-centered k-point mesh with $8 \times 8 \times 6$ k-points for the primitive

four-atom GaN wurtzite cell, which for larger supercells is scaled according to inverse supercell size. LDA, PBE,[76] and HSE06 (Refs. [74] and [75]) XC functionals are employed. In order to reduce the computational effort for HSE06 calculations we follow Ref. [83] and utilize the grid-reduction factor C_i for k-point grid representation of the short-range Fock potential. Based on our tests of the effect of using a grid-reduction factor, we choose to study the band gap of InGaN as a function of In content based on calculations with a grid-reduction factor of 2. This facilitates calculations of alloys, which involve large unit cells to be able to include small fractional In contents. Therefore, the results on alloy band gaps and band-gap bowing are calculated using a grid-reduction factor of 2. In all other cases the reported band gaps have been calculated without grid reduction. For slab calculations we use a grid-reduction factor of 2, i.e., electrostatic potential alignments are calculated using the grid reduction.

PAW potentials that include d electrons as valence electrons are used for Ga and In. The relaxation of the electronic degrees of freedom is stopped when the total-energy change between two consecutive steps is lower than 10^{-4} eV for structure optimizations, or 10^{-6} eV for surface calculations carried out to obtain potential alignments. The relaxation of the ionic degrees of freedom is stopped when the maximum force on one atom is less than 0.02 eV/Å. Whenever results are reported with LDA, PBE, or HSE06 we have used the LDA, PBE, and HSE06 lattice parameters, respectively, unless otherwise noted.

A. Calculations of band alignments

In this section we discuss the scheme used to obtain band alignments. Bulk calculations alone are insufficient to provide band alignments, since they contain no absolute reference for the electrostatic potential.[84] To calculate band alignments, the band structures of the two semiconductors need to be aligned on a common energy scale. This can be accomplished by explicitly modeling an interface between the two materials, which provides an alignment for the electrostatic potentials across the interface.[84,85] In the case of semiconductors which exhibit a significant lattice mismatch, as is the case with AlN, GaN, and InN, such an interface can only be constructed if one or both of the materials is strained in order to provide in-plane lattice matching. The presence of such strains affects the band alignment, and, hence, great care must be taken to properly subtract out these strain effects in order to obtain a so-called "natural band alignment" that would reflect the lineup between unstrained materials.

In order to avoid these complications, we have chosen a different approach, which is actually more appropriate for the problem of surface band alignments that is relevant to water splitting. We have performed surface calculations from which the alignment of the electrostatic potential within the nitride material with respect to the vacuum level can be obtained. By combining surface and bulk calculations, we find the VB and CB positions relative to the vacuum level, i.e., the ionization potential and the electron affinity.

The procedure, therefore, consists of two separate calculations: (i) a bulk calculation to obtain the bulk band structure relative to the average electrostatic potential and (ii) a slab calculation to obtain the difference between the average of the electrostatic potential in the bulk and in vacuum.

B. Bulk and slab supercell size

In order to investigate the electronic structure of InGaN alloys we use 16-atom and 32-atom supercells. The 16-atom supercell allows the metal atoms to have nearest-neighbor coordination numbers corresponding to the average in the random alloy for alloy compositions of 25%, 50%, and 75% and provides a good approximation to the random alloy. This was verified by comparing with special quasirandom structures (SQS). SQS are special types of supercells for which the lattice vectors and structure of the supercell have been chosen such that they provide the best fit to a predefined subset of mth-neighbor pair-correlation functions.[86–88]

We used SQS structures with 32 atoms as developed in Refs. [87] and [88] to investigate the effect of the lack of randomness in the 16-atom supercells. We find the deviation in band gaps to be less than 0.05 eV in the case of 25% In content and smaller than that for 50% In content (0.02 eV) indicating that the 16-atom supercells provide reliable results, comparable to what would be obtained in a fully random model of the alloy.

We use slab calculations to obtain the difference between the average of the electrostatic potential in bulk and in vacuum. The macroscopic and planar-averaged potential of the 12-layer slab are shown in Fig. 1. The planar average of the potential is obtained by averaging potential values within a plane perpendicular to the surface of the slab. The macroscopic average[89] is obtained by taking averages of the planar average potential over distances of one unit cell along the z direction. Ideally slabs should be thick enough to allow the electron density in the center of the slab to be identical to the bulk electron density. We have tested a number of different slab widths and found that for 12-layer slabs (corresponding to three times the alloy bulk unit cell) the bulk-vacuum
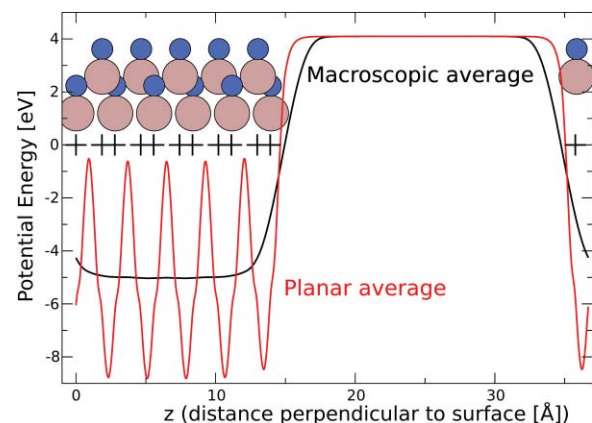

FIG. 1. The macroscopic average (slowly varying black curve) and planar average (oscillating red curve) of the electrostatic potential for an unrelaxed GaN m-plane slab with a width of 12 layers. "+" signs mark the positions of the atomic planes.

electrostatic potential difference is within 0.03 eV of results obtained with very thick slabs (28 layers).

InGaN alloy calculations introduce extra demands on the slab supercells. Our tests show that each layer parallel to the surface plane must have the same cation composition as the bulk alloy, e.g., an $In_{25}Ga_{75}N$ alloy slab must contain one In for every three Ga atoms in each layer. Our tests showed that, if different layers have different compositions (even if the average composition was maintained when averaging over the entire slab), the potential alignment was sensitive to the positioning of the layers within the slab. This is an effect that, in principle, could be eliminated by averaging over a large number of slabs with different arrangements of the planes, but this would be computationally prohibitive. We, therefore, restricted ourselves to slabs in which each plane has the same In composition. In turn, this restricts the In compositions for which we can perform slab calculations, since alloys with small In content lead to very large supercells, which again are computationally prohibitive. As a consequence we restricted the calculations to 0%, 25%, 50%, 75%, and 100% In content.

III. RESULTS AND DISCUSSION

A. Band gaps for binary nitrides

The crystal-field splitting in the wurtzite structure causes a small splitting of the valence bands at the zone center, lifting the threefold degeneracy that would be present in the zinc blende structure. This splitting is highly sensitive to details of the local structure, such as the presence of local strains in an alloy; when investigating band gaps, we, therefore, feel it is more representative to report a value with respect to the *average* value ($E_{v,av}$) of the three valence bands at the Γ point. We will call the resulting band-gap value $E_{g,av}$. The splitting of the bands (due to crystal field, strain, etc.) can subsequently be added back to obtain the actual position of the VBM, E_v, and the corresponding band gap, E_g.

We have tested the effect of varying the HSE06 exact exchange mixing ratio, which is commonly denoted as the parameter α. At 25% mixing we find the following values for $E_{g,av}$: AlN 5.74 eV, GaN 3.23 eV, and InN 0.66 eV. The band gaps with respect to the top valence band, E_g, may be retrieved by subtracting 0.131, 0.004, and 0.022 eV from $E_{g,av}$ AlN, GaN, and InN, respectively. In Fig. 2 the band gaps of AlN, GaN, and InN relative to their respective experimental band gaps are shown as a function of α.

Changing α introduces small changes in the lattice constants, as seen in Table I. The general trend is that higher α leads to smaller lattice constants. The linear correlations seen in Fig. 2 are a combination of the compression of the lattice and the increase in α. We have illustrated this by calculating the band gap of GaN with the lattice constant fixed at the $\alpha = 0.25$ value as seen in Fig. 2. The effect of the compression is also linear but much smaller than the effect of increasing α. The HSE06 default 25% mixing ratio consistently results in too narrow band gaps and mixing in more exact exchange increases the band gap. We find that the mixing ratio required to match the experimental band gaps increases with increasing experimental band gaps such that
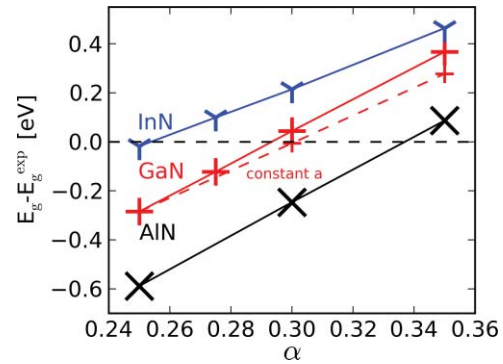

FIG. 2. Difference between calculated (HSE06) band gap E_g and experimental band gap E_g^{exp} [AlN: 6.2 eV (Refs. [2] and [3]), GaN: 3.51 eV (Ref. [4]), InN: 0.65 (Ref. [5])] as a function of α, the exact exchange mixing ratio. The linear fits correspond to AlN: $E_g = 5.61 + 6.753(\alpha - 0.25)$, GaN: $E_g = 3.23 + 6.524(\alpha - 0.25)$, and InN: $E_g = 0.63 + 4.818(\alpha - 0.25)$. The dashed red line is the band gap of GaN with the lattice constants fixed at the $\alpha = 0.25$ values.

AlN requires 33.7%, GaN requires 29.4%, and InN requires 25.4%. It is clear that reproducing the experimental gaps requires different mixing ratios for the different materials. Since in the present study we are calculating properties for alloys, i.e., combinations of two materials, we have chosen to keep α fixed to the default value of 0.25.

B. Band bowing of InGaN alloys

The band gap of InGaN as a function of In content is of key importance for the analysis and design of efficient devices. In light emitters, the band gap of the active layer determines the wavelength of the emitted light, and bowing may affect VB and CB offsets which in turn determine carrier confinement. For application of InGaN in multijunction photovoltaic devices, high efficiency requires that each

TABLE I. AlN, GaN, and InN lattice constants and band gaps.

		LDA	PBE	HSE06 $\alpha = 0.25$	HSE06 $\alpha = 0.30$	HSE06 $\alpha = 0.35$	Expt.[a]
AlN	a	3.09	3.13	3.103	3.097	3.093	3.11
	c/a	1.61	1.61	1.607	1.608	1.608	1.60
	u	0.381	0.381	0.381	0.381	0.381	0.382
	E_g	4.39	4.02	5.61	5.95	6.29	6.1–6.2[b]
	$E_{g,av}$	4.50	4.13	5.74	6.08	6.42	
GaN	a	3.15	3.21	3.181	3.177	3.173	3.19
	c/a	1.63	1.63	1.626	1.623	1.621	1.63
	u	0.376	0.376	0.377	0.378	0.378	0.377
	E_g	2.09	1.69	3.23	3.55	3.88	3.51[c]
	$E_{g,av}$	2.11	1.70	3.23	3.55	3.89	
InN	a	3.51	3.59	3.548	3.543	3.540	3.54
	c/a	1.62	1.62	1.621	1.618	1.614	1.61
	u	0.379	0.378	0.378	0.379	0.380	
	E_g	-0.25	-0.42	0.63	0.86	1.11	0.6–0.7[d]
	$E_{g,av}$	-0.24	-0.40	0.66	0.88	1.12	

[a]Lattice parameters compiled from Refs. [109]–[112].
[b]References [1], [2], and [3].
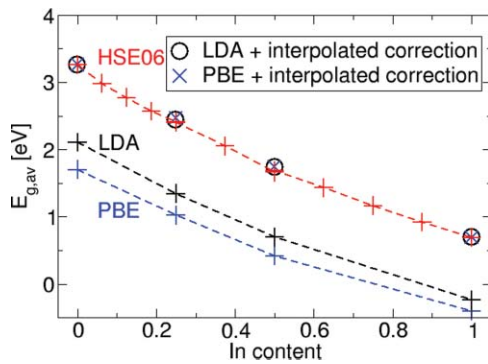[c]Reference [4].
[d]References [5]–[9].

FIG. 3. Band gaps $E_{g,av}$ calculated with HSE06, LDA, and PBE functionals. The "LDA (or PBE) + interpolated correction" data points have been obtained by using the alloy band gaps calculated with LDA/PBE and a correction based on linear interpolation between band-gap corrections for the binaries. The dotted lines connect the data points and are included to guide the eye.

individual junction has a particular band gap.[90] For high efficiency photochemical electrodes, the band gap should satisfy a criterion similar to that for single-junction photovoltaic devices in that the absorbed portion of the solar spectrum should be maximized, with the additional criterion that the band gap should be sufficiently wide to overcome the overpotential of water splitting on the semiconductor or cocatalyst. Accurate information of the band gap of InGaN alloys is, thus, of great importance.

The band gap of InGaN alloys as a function of In content calculated with the LDA, PBE, and HSE06 XC functionals is shown in Fig. 3. We also show results of an approximate interpolation scheme, based on alloy band gaps obtained with LDA or PBE results, corrected by using a linear interpolation of the difference between HSE06 and PBE or LDA results for the binaries. This approximation can be expressed as (for the case of PBE)

$$
\begin{aligned}
E_g(x) = {} & (1-x)[E_g(\text{GaN, HSE}) - E_g(\text{GaN, PBE})] \\
& + x[E_g(\text{InN, HSE}) - E_g(\text{InN, PBE})] \\
& + E_g(\text{In}_x\text{Ga}_{1-x}\text{N, PBE}). \quad (2)
\end{aligned}
$$

There is good agreement between band gaps calculated with HSE06 and the interpolated band gaps (see Fig. 3), with only a slight overestimation of the band-gap values (of the order of 0.05 eV). The close agreement between HSE06 and interpolated band gaps indicates that the widely used approach of using PBE or LDA results for alloys plus a band-gap correction based on linear interpolation between the band-gap corrections ($E_g^{exp} - E_g^{PBE/LDA}$) for the binaries is to a large degree justified.

The band gap of alloys is often reported using a single bowing parameter b calculated by fitting (1). When we force a quadratic fit to $E_{g,av}$ over the entire range of alloy composi-

tions ($0 < x < 1$), we obtain a bowing parameter $b_{av} = 1.10$. The bowing becomes stronger when calculated for the topmost valence band. The position of the top VB E_v relative to $E_{v,av}$ is given by

$$
E_v - E_{v,av} = 0.004\,(1-x) + 0.022x + 0.260x\,(1-x) \ \text{eV}, \tag{3}
$$

which has been obtained by a fit to VB positions calculated using the dense k-point grid (no grid-reduction factor). Thus, the bowing parameter for the top valence band E_v is $b = 1.10 + 0.26 = 1.36$ eV. A recent hybrid functional study based on the PBE0 XC functional found a slightly larger bowing parameter of 1.63 eV; however, the authors do note that PBE0 gives too wide band gaps in the low In region and that this likely leads to a too large bowing parameter.[73]

Furthermore, as has been noted before,[48,91] we find that the bowing at low In content is much stronger than the "global bowing," indicating that a single bowing parameter is unable to accurately describe nonlinearities over the entire composition range. Evaluating the bowing parameter b at specific alloy compositions (see Table II), we find $b = 2.29$ eV at 6.25% and $b = 1.79$ eV at 12.5% based on the top valence band. At intermediate values of alloy composition, we suggest using linear interpolation to estimate b. For instance, at 10% In content we estimate a bowing of 1.99 eV based on the values in Table II. Reference 91 reported band-gap values for well characterized samples in the low In-content region. In order to extract a bowing parameter, the effects of strain need to be subtracted, and a value for the InN band gap needs to be assumed. We have reanalyzed the data of Ref. 91 using more recent values for deformation potentials (Ref. 92) and for the InN band gap (0.65 eV), finding a bowing of 1.97 eV at 10% In content, in excellent agreement with our calculated value of b. Reference 48 reported a strong bowing, in good agreement with Ref. 91 and consequently also in good agreement with the present results. The good agreement with experimental studies, in addition to our tests comparing to SQS structures, indicates that the ordered structures investigated in the present study are an adequate model for the alloy. The low In-content range is currently of highest interest for LED and laser devices, and use of a composition-dependent bowing parameter is, thus, advisable.

C. Calculating band alignments

We calculate band alignments using the approach described in Sec. II. The position of bulk bands are aligned based on the bulk-vacuum potential difference obtained from slab calculations. The accuracy of the applied scheme is evaluated by investigating the following issues: the influence of the amount of exact exchange mixing ratio; the influence of different XC functionals; the difference between the $(1\bar{1}00)$

TABLE II. Bowing parameter as a function of In content.

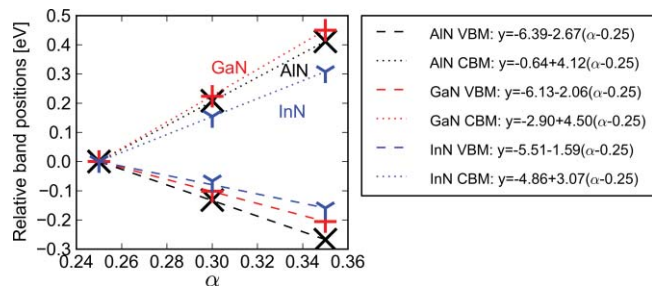| In content	6.25%	12.50%	18.75%	25.00%	37.50%	50.00%	62.50%	75.00%	87.50%
b (eV)	2.29	1.79	1.64	1.39	1.32	1.44	1.22	1.16	1.14

FIG. 4. Change in valence- and conduction-band positions ($E_{v,av}$) relative to the 25% exact exchange value as a function of the amount of exact exchange, α. Equilibrium lattice parameters corresponding to each α value were used, and the atomic positions in the slab were unrelaxed. The legend includes equations to interpolate the band alignment with reference to vacuum for any exact exchange mixing ratio.

m-plane or ($11\bar{2}0$) a-plane orientations; and the effect of relaxing the surface layers.

1. VBM and CBM positions as a function of exact exchange mixing ratio α

As shown in Fig. 2, we established that the band gap is a linear function of exact exchange mixing ratio α. Bulk calculations, however, do not provide information about how the position of the VBM and CBM, individually, changes as a function of the exact exchange mixing parameter. By combining the bulk calculation with slab calculation, we have calculated the band positions as a function of α for AlN, GaN, and InN (see Fig. 4).

Changing α affects the equilibrium lattice parameters (see Table I), and, therefore, we make sure to calculate the

band positions using the self-consistent lattice parameters corresponding to each value of α. The surface calculations in these tests are performed for slabs with all atoms fixed in the bulk geometry, i.e., no surface relaxations are included. It is seen in Fig. 4 that as α increases the VBM moves down and the CBM moves up as a linear function of α. The slopes for the CBM are larger than those for the VBM; thus, the CBM is a stronger function of α than the VBM. It should also be noted that the dependence on α is not the same for each of the binary nitrides.

2. A comparison of LDA, PBE, and HSE06 valence-band positions

Prior studies of group III nitrides have been based on the PBE or the LDA XC functionals, and, therefore, a comparison between the results obtained with these two functionals and HSE06 is appropriate. Figure 5(a) shows that the valence-band position relative to the vacuum level has distinctly different values depending on which XC functional is used. In all cases the equilibrium lattice parameters consistently obtained for each XC functional are used, and the atomic positions are unrelaxed (i.e., fixed in the bulk geometry). The VBM moves down in energy from PBE to LDA to HSE, and the variation from one XC functional to another is largest for AlN and smallest for InN. Thus, the VBM moves down in energy when the XC functional gives a wider band gap (see Table I) and the variation in VBM position is largest for the nitride with the widest band gap, i.e., AlN.

In many cases one is more concerned with the changes in band position from one nitride to the next, i.e., the band offsets. In those cases the "absolute" position of the bands (with
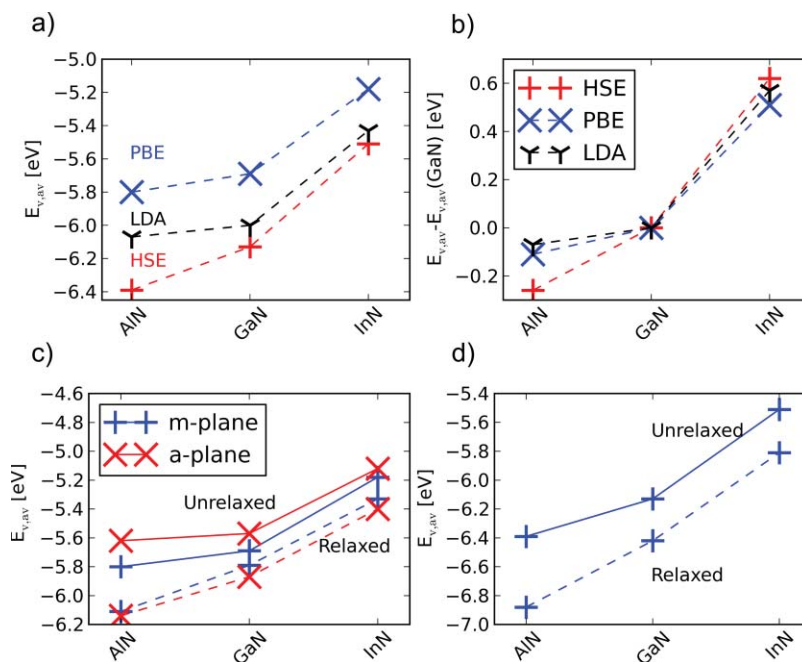

FIG. 5. (a) Valence-band positions ($E_{v,av}$) with respect to the vacuum level for AlN, GaN, and InN calculated for unrelaxed m-plane slabs. Lattice parameters are optimized consistently with the corresponding XC functional (e.g., the PBE values are obtained with lattice parameters optimized with PBE). (b) Same data as in (a), but expressed relative to the GaN VB position. (c) The effect of relaxation on the position of $E_{v,av}$ calculated for relaxed and unrelaxed surfaces of AlN, GaN, and InN using the PBE functional with lattice parameters optimized with PBE. (d) The effect of relaxation on the position of $E_{v,av}$ calculated for relaxed and unrelaxed surfaces of AlN, GaN, and InN using the HSE06 functional with lattice parameters optimized with HSE06.

TABLE III. Valence-band position $E_{v,av}$ calculated with PBE and HSE06 for unrelaxed and relaxed m- and a-plane surfaces. Δ denotes the difference between relaxed and unrelaxed results.

	PBE: m-plane			PBE: a-plane			HSE: m-plane		
	Unrelaxed	Relaxed	Δ	Unrelaxed	Relaxed	Δ	Unrelaxed	Relaxed	Δ
AlN	−5.80	−6.11	−0.31	−5.62	−6.14	−0.52	−6.39	−6.88	−0.50
GaN	−5.69	−5.79	−0.10	−5.57	−5.87	−0.30	−6.13	−6.42	−0.28
InN	−5.18	−5.33	−0.15	−5.12	−5.40	−0.29	−5.51	−5.81	−0.29

respect to the vacuum level) is less relevant, and only the relative positions enter. Figure 5(b) shows the valence-band alignment referenced to the VB in GaN. We observe that LDA and PBE give very similar offsets, and the HSE offsets are only slightly larger (the difference is of the order of 0.1 eV). This variation between the different XC functionals is considerably smaller than the variations observed in the VB positions relative to vacuum seen in Fig. 5(a). This indicates that estimates of relative band alignments can be obtained using LDA or GGA; however, in order to obtain more accurate results HSE06 is needed. Interestingly our HSE06 results show similar trends as GW calculations[43] which also find larger band offsets than LDA and GGA.

3. Effects of surface orientation and relaxations

Calculations of band alignment are complicated by the existence of surface or interface dipoles, which affect slab calculations as well as solid–solid interface calculations. In the case of slab calculations for nonpolar surface planes, the two sides of the slab are identical and surface dipoles will, therefore, be mirror images of each other, ensuring that no potential difference will occur between the two sides of the slab (i.e., no electric field within the slab). However, surface dipoles may shift the bulk-vacuum potential difference. Even though one cannot calculate the absolute magnitude of surface dipoles (due to the lack of a reference), it is of interest to investigate scenarios where the dipoles change. One case of interest is the difference between the nonpolar m- and a-plane surfaces, since different surface planes may have different surface dipoles. Furthermore, we investigate the effect of relaxing the atomic positions in the surface planes, which may also influence surface dipoles.

We find that when the slabs are unrelaxed, i.e., with atomic positions fixed in the bulk structure, the difference between m- and a-plane is largest for AlN (0.19 eV) followed by GaN (0.12 eV) and InN (0.07 eV) [see Fig. 5(c) and Table III], indicating that the surface dipoles on the m- and a-plane are slightly different. Allowing the outermost four layers to relax (on both sides of the slab) leads in all cases to a lowering of the VBM [see Fig. 5(c) and Table III] relative to the unrelaxed surfaces. The lowering of the VBM due to relaxation is largest for the a-plane and the overall effect of including relaxations is to decrease the difference between the VB positions calculated using the m- and a-plane to less than 0.1 eV (see Table III).

This is reassuring and suggests that VB positions obtained from slab calculations for nonpolar wurtzite nitride sur-

faces are representative of some kind of intrinsic alignment, which should, therefore, also be applicable to the problem of band offsets at nitride interfaces.

Finally, we investigate the effect of relaxations depending on which functional (PBE or HSE06) is used. The calculated positions of the VBM obtained using the m-plane with and without relaxations are seen in Fig. 5(d) and tabulated in Table III. Comparing Figs. 5(c) and 5(d), it is seen that relaxations calculated with HSE06 result in larger shifts in band positions than when they are calculated with PBE. Our investigation of the atomic structure indicated that the atomic relaxations calculated with HSE06 are virtually identical to those calculated with PBE; the effect on the VB positions must, therefore, be an electronic structure effect, not attributable to differences in atomic structure.

4. Schemes to reduce the number of hybrid functional calculations

The goal of the present study is not only to investigate binary nitrides but also ternary nitrides, and for these much larger unit cells are required. Systematic use of HSE06 is prohibitively expensive for these larger unit cells. We have, therefore, tested a number of schemes in which parts of the calculations are performed using PBE instead of HSE06.

In Fig. 6 we use the notation "Bulk A/B Surface A/B" where A is the XC functional used to calculate the electronic structure (band structure, electrostatic potential) and B is the XC functional on which the lattice parameters are based. For instance, the cyan-colored line with the label "Bulk: HSE/HSE Surface PBE/HSE" in Fig. 6 is obtained based on bulk band structure calculations, using the HSE06 XC functional performed at the HSE06 lattice parameters, and slab calculations, using the PBE XC functional with HSE06 lattice parameters, thus, consistently using the HSE06 lattice parameters in both bulk and surface calculations.

In Fig. 6(a) the results of the different schemes are all given relative to results obtained with HSE06 throughout (i.e., "Bulk HSE/HSE Surface HSE/HSE"). Figure 6(a) shows that obtaining reliable values relative to vacuum requires the consistent use of HSE06 for the electronic structure calculations of both bulk and surface. Interestingly, the "Bulk HSE/PBE Surface HSE/PBE" scheme (black line) produces results that agree with "Bulk HSE/HSE Surface HSE/HSE" to within 0.05 eV. This result is reassuring, since this shift should be determined by the absolute deformation potential of the VBM, which is quite small (in nitrides[31] as well as other semiconductors[93]) and, hence, only small shifts are expected
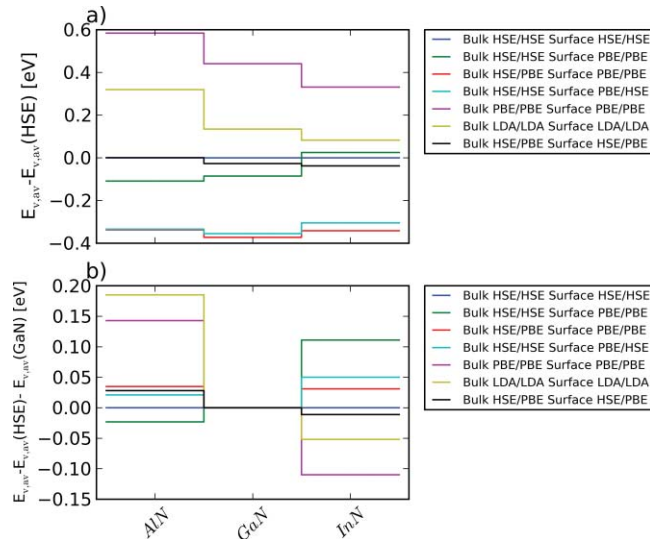
FIG. 6. (a) Valence-band positions ($E_{v,av}$) for unrelaxed structures, relative to HSE values and (b) valence-band alignments ($E_{v,av}$) for unrelaxed structures relative to HSE values, all expressed relative to the $E_{v,av}$ of GaN. The label notation is as follows—Bulk: (XC functional in electronic structure calculation)/(XC functional used to determine lattice parameters), Surface: (XC functional used in electronic structure calculation)/(XC functional used to determine lattice parameters).

since the difference in lattice constant between HSE and PBE is modest (Table I).

All other schemes included in Fig. 6(a) lead to VB positions that differ by at least 0.3 eV for at least one of the three materials. The only exception is the Bulk HSE/HSE Surface PBE/PBE scheme (green line). However, we believe the agreement is fortuitous since this scheme is based on an inconsistent use of lattice parameters (PBE for the surface calculations, HSE for bulk).

Figure 6(b) displays the data shown in the upper part, but now expressed relative to the GaN $E_{v,av}$, thus, making it clearer which approximate scheme works better (i.e., is closest to "Bulk HSE/HSE Surface HSE/HSE") for *relative* band alignments. Figure 6(b) indicates that *relative* band alignments (i.e., referenced to the VB of GaN) are given with much higher accuracy when certain approximate schemes are used. Again, we feel it is important to use the same lattice parameters for the bulk and slab calculations. Good results (less than 0.05 eV deviation from HSE06) may be obtained by using HSE06 for the bulk calculation with the HSE06 lattice parameters and PBE for the slab calculation with the HSE06 lattice parameters (cyan line). Alternatively, using HSE06 for the bulk calculation with the PBE lattice parameters and PBE for the slab calculation with the PBE lattice parameters (red line) also produces good results. But note that the corresponding $E_{v,av}$ positions with respect to vacuum [Fig. 6(a)] are shifted by more than 0.3 eV compared to the most accurate values.

We have also performed tests similar to those shown in Fig. 6 for relaxed surfaces. These show that, once again, "Bulk HSE/HSE Surface HSE/HSE" and "Bulk HSE/PBE Surface HSE/PBE" calculations produce very similar VB positions (to within 0.05 eV). However, in both cases the electronic structure calculation for the surface is still carried out using HSE, and thus very expensive.

We now turn to the question of how to treat the effect of surface relaxations without doing full-fledged HSE06 calculations for the surface. It is clear from Figs. 5(c) and 5(d) that simply using PBE to calculate the effect of relaxations is not a good approximation to the full HSE06 result. Qualitatively, a downshift of the $E_{v,av}$ is observed when relaxations are included in both PBE and HSE, but quantitatively the shift is too small in PBE. In the case of m-plane InGaN alloys, we have calculated the effect of relaxations using the PBE XC functional at the PBE lattice parameters. We find that relaxations move $E_{v,av}$ down by 0.055, 0.070, and 0.085 eV for In contents of 25%, 50%, and 75%, respectively. Comparing these values with linear interpolation from GaN to InN gives a mean absolute error of 0.05 eV. We suggest here that linear interpolation of relaxation effects based on HSE06 is reliable to within a similar error bar, based on the fact that the difference between Δ (Table III) obtained in HSE versus PBE is very similar for the two binaries (0.19 eV for GaN and 0.15 eV for InN).

We have, additionally, performed tests with the following procedure: "Bulk: HSE/PBE" combined with an HSE electronic structure calculation of the surface relaxed with PBE at the PBE lattice constant. This produces results in very good agreement (differences less than 0.05 eV) with "Bulk: HSE/HSE Surface: HSE/HSE (relaxed)" calculations. The approach in which relaxations are calculated using PBE is less expensive than the full HSE calculation, but still too computationally demanding to be carried out systematically for a range of alloy compositions. Future increase in computer power may make this a viable approach, though.

To summarize, we find that for binary nitrides both the bulk and the slab calculations should be performed consistently with HSE06. In the case where brute force HSE06 calculations are not feasible (i.e., slab calculations for ternary nitrides) or when time is a priority (initial screening studies), the following procedure is recommended: (i) bulk calculation with HSE06 at the HSE06 lattice parameters; (ii) unrelaxed slab calculations with the PBE XC functional at the HSE06 lattice parameters; and (iii) including relaxation effects by linear interpolation between binary nitride values calculated using HSE06.

D. Electron affinities and band offsets of binary nitrides

1. Electron affinities and ionization potentials of binary nitrides

For GaN, we calculate an electron affinity of 3.18 eV for the relaxed surface (2.90 eV for unrelaxed), which falls within the range of 2.6 to 3.5 eV reported in a number of experimental studies.[94–99] The calculated electron affinity for AlN is 1.01 eV for relaxed surfaces (0.52 eV for unrelaxed), which is again within the range of reported experimental values [0.25 ± 0.3 eV,[100] 1.9 eV,[101] and 0 eV (Ref. 99)]. It should be kept in mind that experimental measurements may include the effects of adsorbates on the surface; in particular, aluminum nitride surfaces are easily oxidized[102, 103] and the presence of an oxide layer may affect the band alignment.[99, 101]
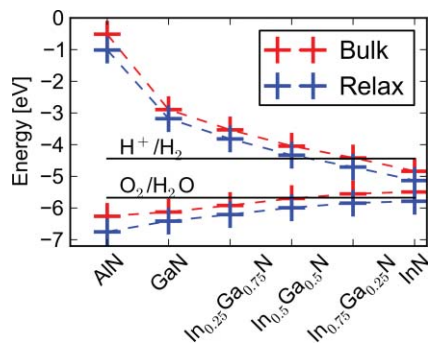
FIG. 7. Valence-band (E_v) and conduction-band positions referenced to the vacuum level calculated for relaxed and unrelaxed surfaces. H^+/H_2 is the redox potential for hydrogen evolution and O_2/H_2O is the redox potential for oxygen evolution. The binary nitride results consistently use the HSE06 functional in bulk and surface calculations. The results for ternary InGaN alloys are based on HSE06 bulk calculations and surface calculations with PBE at the HSE lattice parameters. Effects of relaxation are included by linear interpolation between GaN and InN.

For photochemical hydrogen production the band gap must, at a minimum, straddle the redox potentials of water and hydrogen evolution. Experimentally the position of the VBM and CBM relative to the standard hydrogen electrode (SHE) is measured by capacitance or photocurrent measurements.[104] Both methods lead to a value for the flat-band potential relative to a reference electrode. Electron affinities may be linked to flat-band potentials, based on the difference in energy from the Fermi energy to the CBM in the bulk of the semiconductor and the band offset due to the semiconductor/electrolyte interface.[104] Calculating the latter is one of the key challenges in theoretical electrochemistry[105] and beyond the scope of the present study. Here we neglect the effect of the semiconductor/electrolyte interface, and assume the SHE to be at -4.44 eV relative to vacuum,[106] which leads to a redox potential of oxygen evolution at -5.67 eV (-1.23 eV relative to SHE) at standard conditions (see Fig. 7). We, thus, find the GaN CBM to be 1.26 eV above the redox potential of hydrogen evolution.

2. Band offsets of binary nitrides

We calculate band offsets based on electron affinities and ionization potentials for the nonpolar surfaces. The similarity of the results for the relaxed m- and a-plane surfaces suggests that the inclusion of relaxations is most appropriate to obtain natural band alignments.

For InN/GaN we find 0.62 eV, while for AlN/GaN we find 0.34 eV, and finally for AlN/InN we find 0.96 eV. For InN/GaN our result is very close to the most recent experimental result of 0.58 ± 0.08 eV (Ref. 28) and slightly larger than previous LAPW calculations [0.48 eV (Ref. 29)]. Care should be taken when comparing to experimentally measured band offsets because the overlayer may be strained. Even though the overlayers of InN on GaN in Ref. 28 were very thin (5 nm), the authors state that due to the extremely large lattice mismatch between GaN and InN the majority of the strain relaxes within the first few monolayers of growth and, therefore, strain does not affect the measured VBO. The mea-

sured offsets should, therefore, be representative of the natural band alignment calculated in the present study. Calculations based on the PBE0 hybrid functional found a much larger InN/GaN offset of $\sim$1.9 eV.[73] However, the band offset in Ref. 73 is based on the average electrostatic potential without any external reference such as an interface or a surface. One may speculate that this lack of a proper reference[84] is the cause of the very large InN/GaN band offset found in Ref. 73.

For AlN/GaN the offset of 0.34 eV falls within the (very wide) range of experimentally measured values [0.15 to 1.4 eV (Refs. 33–35 and 106)] and is somewhat smaller than previous theoretical calculations which reported 0.7–1.6 eV.[29,31,36–44,108] For AlN/InN we report 0.96 eV which is also smaller than the reported experimental offset of 1.52 eV.[109]

Slightly larger band offsets are obtained if one uses the α value (amount of exact exchange mixed in) which gives the experimental band gap (AlN: 6.2 eV, GaN: 3.51 eV, InN: 0.65 eV), as found in Fig. 2 (AlN: 33.7%, GaN: 29.4%, InN: 25.4%). Combined with the linear interpolation of the band positions from Fig. 4 and the effect of relaxation obtained with $\alpha = 0.25$, this results in band offsets (for the average valence bands) of 0.48 eV for AlN/GaN and 0.71 eV for InN/GaN. For the valence-band maximum, the corresponding values are 0.43 eV for AlN/GaN and 0.70 eV for InN/GaN.

E. Electron affinities and ionization potentials for InGaN alloys

Designing heterostructures and photochemical electrodes requires that the band positions of the individual materials can be accurately predicted. The calculated positions of the CBM and VBM relative to vacuum are shown in Fig. 7. We have used the three-step process outlined at the end of Sec. III B. The three-step process allows us to include the InGaN alloys with 25%, 50%, and 75% In content and include the effect of relaxing the surface layers.

In order for InGaN to be an appropriate semiconductor for water splitting, the VBM and CBM must at least straddle the redox potential of hydrogen and oxygen evolution. Based on this minimum criterion we find that the CBM of InGaN crosses the redox potential at $\sim$50% In content, above which InGaN will no longer be able to drive the hydrogen evolution reaction.

Our results for InGaN alloys allow us to investigate how the band-gap bowing is distributed over the VB and the CB. We find that the bowing originates almost entirely from the CB (see Fig. 7). E_v has a small upward bowing (see Fig. 7), while $E_{v,av}$ varies linearly from GaN to InN with a slope of $0.62x$, where x is the In content. This result is in reasonable agreement with experiments that also report a linear dependence of E_v on In content in the 0–0.3 range,[108] but find a slightly higher slope $(0.85 \pm 0.15)x$. The slight amount of bowing of E_v is a result of the bowing of E_v relative to $E_{v,av}$ [Eq. (3)]. Thus, our results put the commonly used approximation in which all the bowing is attributed to the CB on much firmer ground.

IV. CONCLUSION

We have investigated the band gaps and band alignments of AlN, GaN, InN, and InGaN alloys using density functional theory with the LDA, PBE, and HSE06 XC functionals. We find that HSE06 significantly improves the accuracy of calculated band gaps compared to the LDA and PBE, even if it slightly underestimates the band gap compared to experimental values. The band gap calculated with HSE06 does depend on the amount α of exact exchange mixed in and we find a linear dependence on α. However, no single mixing ratio reproduces the experimental gap for all nitrides. We have also investigated the band gap of InGaN alloys using HSE06 and find a significant bowing at low In contents; the bowing cannot accurately be described by a composition-independent bowing parameter. Finally, band gaps calculated with PBE or LDA lead to the same bowing of the band gap, and the band gap of InGaN alloys may, therefore, be obtained from PBE or LDA calculations for the alloy, combined with a linear interpolation of the band-gap corrections for binary GaN and InN.

Electron affinities and ionization potentials change dramatically when calculated with HSE06 compared to LDA and PBE. However, relative band alignments are less sensitive to the choice of XC functional than electron affinities and ionization potentials. We find that electron affinities for the nonpolar m- and a-plane are similar when relaxations are included. These results for binaries may be combined with results for alloys to calculate alloy band alignments using the following approach: (i) bulk calculation with HSE06 at the HSE06 lattice parameters; (ii) unrelaxed slab calculations with the PBE XC functional at the HSE06 lattice parameters; and (iii) including relaxation effects by linear interpolation between binary nitride values calculated using HSE06.

We find that the average valence band ($E_{\mathrm{v,av}}$) of InGaN is a linear function of In content and that virtually all of the bowing in the band gap originates from bowing in the conduction band, with a small amount of VB bowing due to the bowing of the VBM with respect to $E_{\mathrm{v,av}}$.

GaN and InGaN are being considered as materials for photochemical electrodes for water splitting, and based on our calculated band alignments we predict that InGaN will be able to split water up to 50% In content.

ACKNOWLEDGMENTS

[1] J. Li, K. B. Nam, M. L. Nakarmi, J. Y. Lin, H. X. Jiang, P. Carrier, and S. H. Wei, Appl. Phys. Lett. **83**, 5163 (2003).

[2] H. Yamashita, K. Fukui, S. Misawa, and S. Yoshida, J. Appl. Phys. **50**, 896 (1979).

[3] D. Brunner, H. Angerer, E. Bustarret, F. Freudenberg, R. Hopler, R. Dimitrov, O. Ambacher, and M. Stutzmann, J. Appl. Phys. **82**, 5090 (1997).

[4] I. Vurgaftman and J. R. Meyer, J. Appl. Phys. **94**, 3675 (2003).

[5] C. S. Gallinat, G. Koblmuller, J. S. Brown, S. Bernardis, J. S. Speck, G. D. Chern, E. D. Readinger, H. G. Shen, and M. Wraback, Appl. Phys. Lett. **89**, 032109 (2006).

[6] J. Wu, W. Walukiewicz, W. Shan, K. M. Yu, J. W. A. III, S. X. Li, E. E. Haller, H. Lu, and W. J. Schaff, J. Appl. Phys. **94**, 4457 (2003).

[7] M. Higashiwaki and T. Matsui, J. Cryst. Growth **269**, 162 (2004).

[8] T. Araki, Y. Saito, T. Yamaguchi, M. Kurouchi, Y. Nanishi, and H. Naoi, J. Vac. Sci. Technol. B **22**, 2139 (2004).

[9] K. M. Yu, Z. Liliental-Weber, W. Walukiewicz, W. Shan, J. W. Ager, S. X. Li, R. E. Jones, E. E. Haller, H. Lu, and W. J. Schaff, Appl. Phys. Lett. **86**, 071910 (2005).

[10] C. J. Neufeld, N. G. Toledo, S. C. Cruz, M. Iza, S. P. DenBaars, and U. K. Mishra, Appl. Phys. Lett. **93**, 143502 (2008).

[11] R. Dahal, B. Pantha, J. Li, J. Y. Lin, and H. X. Jiang, Appl. Phys. Lett. **94**, 063505 (2009).

[12] X. Zheng, R.-H. Horng, D.-S. Wuu, M.-T. Chu, W.-Y. Liao, M.-H. Wu, R.-M. Lin, and Y.-C. Lu, Appl. Phys. Lett. **93**, 261108 (2008).

[13] K. Fujii, T. K. Karasawa, and K. Ohkawa, Jpn. J. Appl. Phys. **44**, L543 (2005).

[14] J. Li, J. Y. Lin, and H. X. Jiang, Appl. Phys. Lett. **93**, 162107 (2008).

[15] K. Fujii and K. Ohkawa, J. Electrochem. Soc. **153**, A468 (2006).

[16] K. Fujii, Y. Iwaki, H. Masui, T. J. Baker, M. Iza, H. Sato, J. Kaeding, T. Yao, J. S. Speck, S. P. Denbaars, S. Nakamura, and K. Ohkawa, Jpn. J. Appl. Phys. **46**, 6573 (2007).

[17] K. Fujii, K. Kusakabe, and K. Ohkawa, Jpn. J. Appl. Phys. **44**, 7433 (2005).

[18] K. Fujii, M. Ono, T. Ito, Y. Iwaki, A. Hirako, and K. Ohkawa, J. Electrochem. Soc. **154**, B175 (2007).

[19] M. Ono, K. Fujii, T. Ito, Y. Iwaki, A. Hirako, T. Yao, and K. Ohkawa, J. Chem. Phys. **126**, 054708 (2007).

[20] I. Waki, D. Cohen, R. Lal, U. Mishra, S. P. DenBaars, and S. Nakamura, Appl. Phys. Lett. **91**, 093519 (2007).

[21] G. Martin, A. Botchkarev, A. Rockett, and H. Morkoc, Appl. Phys. Lett. **68**, 2541 (1996).

[22] C.-F. Shih, N.-C. Chen, P.-H. Chang, and K.-S. Liu, Jpn. J. Appl. Phys. **44**, 7892 (2005).

[23] T. Ohashi, P. Holmstrom, A. Kikuchi, and K. Kishino, Appl. Phys. Lett. **89**, 041907 (2006).

[24] C.-L. Wu, H.-M. Lee, C.-T. Kuo, S. Gwo, and C.-H. Hsu, Appl. Phys. Lett. **91**, 042112 (2007).

[25] Z. H. Mahmood, A. P. Shah, A. Kadir, M. R. Gokhale, S. Ghosh, A. Bhattacharya, and B. M. Arora, Appl. Phys. Lett. **91**, 152108 (2007).

[26] K. Wang, C. Lian, N. Su, D. Jena, and J. Timler, Appl. Phys. Lett. **91**, 232117 (2007).

[27] C.-L. Wu, H.-M. Lee, C.-T. Kuo, C.-H. Chen, and S. Gwo, Appl. Phys. Lett. **92**, 162106 (2008).

[28] P. D. C. King, T. D. Veal, C. E. Kendrick, L. R. Bailey, S. M. Durbin, and C. F. McConville, Phys. Rev. B **78**, 033308 (2008).

[29] S.-H. Wei and A. Zunger, Appl. Phys. Lett. **69**, 2719 (1996).

[30] Y. H. Li, A. Walsh, S. Y. Chen, W. J. Yin, J. H. Yang, J. B. Li, J. L. F. Da Silva, X. G. Gong, and S. H. Wei, Appl. Phys. Lett. **94**, 212109 (2009).

[31] C. G. Van de Walle and J. Neugebauer, Appl. Phys. Lett. **70**, 2577 (1997).

[32] W. Monch, J. Appl. Phys. **80**, 5076 (1996).

[33] A. Rizzi, R. Lantier, F. Monti, H. Luth, F. Della Sala, A. Di Carlo, and P. Lugli, J. Vac. Sci. Technol. B **17**, 1674 (1999).

[34] Z. Sitar, M. J. Paisley, B. Yan, R. F. Davis, J. Ruan, and J. W. Choyke, Thin Solid Films **200**, 311 (1991).

[35] J. R. Waldrop and R. W. Grant, Appl. Phys. Lett. **68**, 2879 (1996).

[36] E. A. Albanesi, W. R. L. Lambrecht, and B. Segall, J. Vac. Sci. Technol. B **12**, 2470 (1994).

[37] S. Satpathy, Z. S. Popovic, and W. C. Mitchel, J. Appl. Phys. **95**, 5597 (2004).

[38] M. B. Nardelli, K. Rapcewicz, and J. Bernholc, Phys. Rev. B **55**, R7323 (1997).

[39] N. Binggeli, P. Ferrara, and A. Baldereschi, Phys. Rev. B **63**, 245306 (2001).

[40] F. Bernardini and V. Fiorentini, Phys. Rev. B **57**, R9427 (1998).

[41] J. A. Majewski, G. Zandler, and P. Vogl, Semicond. Sci. Technol. **13**, A90 (1998).

[42]A. Satta, V. Fiorentini, A. Bosin, F. Meloni, and D. Vanderbilt, in *Gallium Nitride and Related Materials. First International Symposium*, edited by F. A. Ponce, R. D. Dupuis, S. Nakamura, and J. A. Edmond [Mater. Res. Soc. Symp. Proc. **395**, 515 (1996)].

[43]D. Cociorva, W. G. Aulbur, and J. W. Wilkins, Solid State Commun. **124**, 63 (2002).

[44]A. Rubio, J. L. Corkill, and M. L. Cohen, Phys. Rev. B **49**, 1952 (1994).

[45]M. D. McCluskey, C. G. Van de Walle, L. T. Romano, B. S. Krusor, and N. M. Johnson, J. Appl. Phys. **93**, 4340 (2003).

[46]J. Wu, W. Walukiewicz, K. M. Yu, J. W. A. III, E. E. Haller, H. Lu, and W. J. Schaff, Appl. Phys. Lett. **80**, 4741 (2002).

[47]S. Pereira, M. R. Correia, T. Monteiro, E. Pereira, E. Alves, A. D. Sequeira, and N. Franco, Appl. Phys. Lett. **78**, 2137 (2001).

[48]C. Wetzel, T. Takeuchi, S. Yamaguchi, H. Katoh, H. Amano, and I. Akasaki, Appl. Phys. Lett. **73**, 1994 (1998).

[49]G. Franssen, I. Gorczyca, T. Suski, A. Kaminska, J. Pereiro, E. Munoz, E. Iliopoulos, A. Georgakilas, S. B. Che, Y. Ishitani, A. Yoshikawa, N. E. Christensen, and A. Svane, J. Appl. Phys. **103**, 033514 (2008).

[50]M. Moret, B. Gil, S. Ruffenach, O. Briot, C. Giesen, M. Heuken, S. Rushworth, T. Leese, and M. Succi, J. Cryst. Growth **311**, 2795 (2009).

[51]R. Kudrawiec, M. Siekacz, M. Krysko, G. Cywinski, J. Misiewicz, and C. Skierbiszewski, J. Appl. Phys. **106**, 113517 (2009).

[52]F. B. Naranjo, M. A. Sanchez-Garcia, F. Calle, E. Calleja, B. Jenichen, and K. H. Ploog, Appl. Phys. Lett. **80**, 231 (2002).

[53]S. Nakamura, J. Vac. Sci. Technol. A **13**, 705 (1995).

[54]Z. Dridi, B. Bouhafs, and P. Ruterana, Semicond. Sci. Technol. **18**, 850 (2003).

[55]B.-T. Liou, C.-Y. Lin, S.-H. Yen, and Y.-K. Kuo, Opt. Commun. **249**, 217 (2005).

[56]C. Caetano, L. K. Teles, M. Marques, J. Pino, A. Dal, and L. G. Ferreira, Phys. Rev. B **74**, 045215 (2006).

[57]M. Ferhat and F. Bechstedt, Phys. Rev. B **65**, 075213 (2002).

[58]L. K. Teles, J. Furthmuller, L. M. R. Scolfaro, J. R. Leite, and F. Bechstedt, Phys. Rev. B **63**, 085204 (2001).

[59]F. Bechstedt, J. Furthmuller, M. Ferhat, L. K. Teles, L. M. R. Scolfaro, J. R. Leite, V. Y. Davydov, O. Ambacher, and R. Goldhahn, Phys. Status Solidi A **195**, 628 (2003).

[60]C. G. Van de Walle, M. D. McCluskey, C. P. Master, L. T. Romano, and N. M. Johnson, Mater. Sci. Eng., B **59**, 274 (1999).

[61]B. Lee and L. W. Wang, J. Appl. Phys. **100**, 093717 (2006).

[62]A. F. Wright and J. S. Nelson, Appl. Phys. Lett. **66**, 3051 (1995).

[63]I. Gorczyca, S. P. Lepkowski, T. Suski, N. E. Christensen, and A. Svane, Phys. Rev. B **80**, 075202 (2009).

[64]I. Gorczyca, T. Suski, N. E. Christensen, and A. Svane, Appl. Phys. Lett. **96**, 101907 (2010).

[65]X. J. Zhu and S. G. Louie, Phys. Rev. B **43**, 14142 (1991).

[66]S. B. Zhang, D. Tomanek, S. G. Louie, M. L. Cohen, and M. S. Hybertsen, Solid State Commun. **66**, 585 (1988).

[67]R. Shaltaf, G. M. Rignanese, X. Gonze, F. Giustino, and A. Pasquarello, Phys. Rev. Lett. **100**, 186401 (2008).

[68]P. Rinke, A. Qteish, J. Neugebauer, C. Freysoldt, and M. Scheffler, New J. Phys. **7**, 126 (2005).

[69]P. Rinke, M. Scheffler, A. Qteish, M. Winkelnkemper, D. Bimberg, and J. Neugebauer, Appl. Phys. Lett. **89**, 161919 (2006).

[70]P. Rinke, M. Winkelnkemper, A. Qteish, D. Bimberg, J. Neugebauer, and M. Scheffler, Phys. Rev. B **77**, 075202 (2008).

[71]A. Schleife, F. Fuchs, C. Rodl, J. Furthmuller, and F. Bechstedt, Phys. Status Solidi B **246**, 2150 (2009).

[72]J. P. A. Charlesworth, R. W. Godby, and R. J. Needs, Phys. Rev. Lett. **70**, 1685 (1993).

[73]X. Wu, E. J. Walter, A. M. Rappe, R. Car, and A. Selloni, Phys. Rev. B **80**, 115201 (2009).

[74]J. Heyd, G. E. Scuseria, and M. Ernzerhof, J. Chem. Phys. **118**, 8207 (2003).

[75]J. Heyd, G. E. Scuseria, and M. Ernzerhof, J. Chem. Phys. **124**, 219906 (2006).

[76]J. P. Perdew, K. Burke, and M. Ernzerhof, Phys. Rev. Lett. **77**, 3865 (1996).

[77]P. G. Moses and C. G. Van de Walle, Appl. Phys. Lett. **96**, 021908 (2010).

[78]S. R. Bahn and K. W. Jacobsen, Comput. Sci. Eng. **4**, 56 (2002).

[79]G. Kresse and J. Hafner, Phys. Rev. B **47**, 558 (1993).

[80]G. Kresse and J. Furthmuller, Phys. Rev. B **54**, 11169 (1996).

[81]G. Kresse and D. Joubert, Phys. Rev. B **59**, 1758 (1999).

[82]P. E. Blochl, Phys. Rev. B **50**, 17953 (1994).

[83]J. Paier, M. Marsman, K. Hummer, G. Kresse, I. C. Gerber, and J. G. Angyan, J. Chem. Phys. **124**, 154709 (2006).

[84]C. G. Van de Walle and R. M. Martin, Phys. Rev. B **35**, 8154 (1987).

[85]A. Franciosi and C. G. Van de Walle, Surf. Sci. Rep. **25**, 1 (1996).

[86]A. Zunger, S. H. Wei, L. G. Ferreira, and J. E. Bernard, Phys. Rev. Lett. **65**, 353 (1990).

[87]D. Shin, R. Arroyave, Z.-K. Liu, and A. V. de Walle, Phys. Rev. B **74**, 024204 (2006).

[88]D. Shin, R. Arroyave, Z.-K. Liu, and A. V. de Walle, Phys. Rev. B **76**, 069901 (2007).

[89]A. Baldereschi, S. Baroni, and R. Resta, Phys. Rev. Lett. **61**, 734 (1988).

[90]S. Kurtz, D. Friedman, J. Geisz, and W. McMahon, J. Cryst. Growth **298**, 748 (2007).

[91]M. D. McCluskey, C. G. Van de Walle, C. P. Master, L. T. Romano, and N. M. Johnson, Appl. Phys. Lett. **72**, 2725 (1998).

[92]Q. M. Yan, P. Rinke, M. Scheffler, and C. G. Van de Walle, Appl. Phys. Lett. **95**, 121111 (2009).

[93]C. G. Van de Walle and R. M. Martin, Phys. Rev. Lett. **62**, 2028 (1989).

[94]S. P. Grabowski, M. Schneider, H. Nienhaus, W. Monch, R. Dimitrov, O. Ambacher, and M. Stutzmann, Appl. Phys. Lett. **78**, 2503 (2001).

[95]C. I. Wu and A. Kahn, J. Vac. Sci. Technol. B **16**, 2218 (1998).

[96]C. I. Wu, A. Kahn, N. Taskar, D. Dorman, and D. Gallagher, J. Appl. Phys. **83**, 4249 (1998).

[97]K. M. Tracy, W. J. Mecouch, R. F. Davis, and R. J. Nemanich, J. Appl. Phys. **94**, 3163 (2003).

[98]V. M. Bermudez, J. Appl. Phys. **80**, 1190 (1996).

[99]M. C. Benjamin, M. D. Bremser, T. W. Weeks, S. W. King, R. F. Davis, and R. J. Nemanich, Appl. Surf. Sci. **104–105**, 455 (1996).

[100]C. I. Wu and A. Kahn, Appl. Phys. Lett. **74**, 546 (1999).

[101]M. S. Miao, A. Janotti, and C. G. Van de Walle, Phys. Rev. B **80**, 155319 (2009).

[102]M. S. Miao, P. G. Moses, J. R. Weber, A. Janotti, and C. G. Van de Walle, EPL **89**, 4 (2010).

[103]A. J. Nozik, Annu. Rev. Phys. Chem. **29**, 189 (1978).

[104]J. Rossmeisl, E. Skulason, M. E. Bjorketun, V. Tripkovic, and J. K. Norskov, Chem. Phys. Lett. **466**, 68 (2008).

[105]S. Trasatti, Pure Appl. Chem. **58**, 955 (1986).

[106]J. Baur, K. Maier, M. Kunzer, U. Kaufmann, and J. Schneider, Appl. Phys. Lett. **65**, 2211 (1994).

[107]P. D. C. King, T. D. Veal, P. H. Jefferson, C. F. McConville, T. Wang, P. J. Parbrook, H. Lu, and W. J. Schaff, Appl. Phys. Lett. **90**, 132105 (2007).

[108]T. Makimoto, K. Kumakura, T. Nishida, and N. Kobayashi, J. Electron. Mater. **31**, 313 (2002).

[109]O. Madelung, *Semiconductors-Basic Data* (Springer, Berlin, 1996).

[110]H. Schulz and K. H. Thiemann, Solid State Commun. **23**, 815 (1977).

[111]W. M. Yim, E. J. Stofko, P. J. Zanzucch, J. I. Pankove, M. Ettenber, and S. L. Gilbert, J. Appl. Phys. **44**, 292 (1973).

[112]H. P. Maruska and J. J. Tietjen, Appl. Phys. Lett. **15**, 327 (1969).